HHS Public Access

Author manuscript

Neuron. Author manuscript; available in PMC 2016 April 08.

Published in final edited form as:

Neuron. 2015 April 8; 86(1): 207–217. doi:10.1016/j.neuron.2015.02.033.

Photosensitivity of neurons enabled by cell-targeted gold nanoparticles

João L. Carvalho-de-Souza[1,*], **Jeremy S. Treger**[1,*], **Bobo Dang**[2,*], **Stephen B. H. Kent**[2], **David R. Pepperberg**[3,‡], and **Francisco Bezanilla**[1,‡]

[1]Department of Biochemistry and Molecular Biology, University of Chicago, Chicago, IL 60637, USA

[2]Department of Chemistry, University of Chicago, Chicago, IL 60637, USA

[3]Lions of Illinois Eye Research Institute, Illinois Eye and Ear Infirmary, Department of Ophthalmology and Visual Sciences, University of Illinois at Chicago, Chicago, IL 60612, USA

Summary

Unmodified neurons can be directly stimulated with light to produce action potentials, but such techniques have lacked localization of the delivered light energy. Here we show that gold nanoparticles can be conjugated to high-avidity ligands for a variety of cellular targets. Once bound to a neuron, these particles transduce millisecond pulses of light into heat which changes membrane capacitance, depolarizing the cell and eliciting action potentials. Compared to non-functionalized nanoparticles, ligand-conjugated nanoparticles highly resist convective washout, and enable photothermal stimulation with lower delivered energy and resulting temperature increase. Ligands targeting three different membrane proteins were tested; all showed similar activity and washout resistance. This suggests that many types of ligands can be bound to nanoparticles, preserving ligand and nanoparticle function, and that many different cell phenotypes can be targeted by appropriate choice of ligand. The findings have applications as an alternative to optogenetics, and potentially for therapies involving neuronal photostimulation.

‡To whom correspondence should be addressed. fbezanilla@uchicago.edu, davipepp@uic.edu.
*Co-first Authors

Supplemental Information

Supplemental Information includes eight figures and Supplemental Experimental Procedures, and it can be found with this article online at XXXXX.

Author Contributions

The project was conceived by D.R.P. and F.B. All authors contributed to design of the research. J.L.CdS performed the patch clamp and bilayer experiments, with close assistance by J.S.T. J.S.T. and J.L.CdS performed the brain slice imaging experiments. J.L.CdS, J.S.T., and F.B. analyzed the electrophysiological data. S.B.H.K and B.D. designed, and B.D. performed, the chemical syntheses. F.B. and J.S.T. developed and carried out the computational modeling. J.S.T. and J.L.CdS wrote the manuscript, with assistance by D.R.P. and F.B.

Introduction

Selective optical stimulation of specific classes of excitable cells is a major goal in neurobiology. Optical stimulation avoids many of the problems inherent to electrodes, such as invasiveness and lack of specificity, and can thus allow for novel experimental designs. A common method to achieve this optical stimulation is through optogenetics, wherein molecules such as channelrhodopsin are selectively expressed in different cell types; exposure to light opens these channels and causes cell depolarization (Packer et al., 2013; Zhang et al., 2006). While this technique is undoubtedly powerful, it requires gene transfection to achieve cellular expression of the light-sensitive proteins. As such, it is not currently suitable for use in a variety of systems including human subjects, where gene therapy remains highly experimental (Ginn et al., 2013).

One potential alternative to optogenetic techniques is the direct optical stimulation of unmodified neurons (Allègre et al., 1994; Hirase et al., 2002; Lugo et al., 2012). Direct optical stimulation approaches have included the use of infrared (IR) (Wells et al., 2005) wavelengths, although the mechanism of this effect was not initially understood. Recently, Shapiro and collaborators (Shapiro et al., 2012) showed that for IR wavelengths, laser-induced fast changes in the temperature of the local aqueous medium can heat the cell membrane and produce capacitive currents. Further experimentation and modeling demonstrated that changes in the cells' membrane capacitances were sufficient to produce the observed depolarizing currents and action potentials under physiological conditions. However, while direct heating of bulk solution with IR light is effective, it is an imprecise way to stimulate neurons and may cause off-target effects or cellular damage.

Gold nanorods (AuNRs) have been investigated as a more targeted alternative due to their ability to absorb NIR light and efficiently convert this energy to heat. This heating effect has a short range, and since NIR light is not strongly absorbed by water, the bulk aqueous media is unaffected. AuNR heating has been used to excite cultured neurons and exposed nerves by depositing the rods in proximity to cell membranes (Eom et al., 2014; Yong et al., 2014). Spherical gold nanoparticles (AuNPs) with a 20 nm diameter are similar to AuNRs in that they can absorb light and convert this energy to heat (Roper et al., 2007), but their plasmon absorption band exhibits a peak near 523 nm rather than in the NIR range. The relatively strong absorbance of the 20 nm spherical AuNPs at 523 nm, i.e., at wavelengths typically prominent in indoor as well as daylight ambient illumination, suggests that photothermal neuronal excitation mediated by these AuNPs might have utility for applications such as the restoration of light-induced signaling within the retina of patients with photoreceptor degenerative disease. However, while the short-range heating effect of AuNPs and AuNRs allows for selective heating of a localized environment, it also has a significant drawback: the particles must be extremely close to the cells of interest in order to produce any effect.

Here we report an approach of potentially wide applicability for highly localized AuNP-mediated photostimulation of neurons by conjugating the AuNPs to functional groups that specifically bind to external motifs of neuronal membrane proteins. Similar strategies have previously been used to target nanoparticles to cancer cells to facilitate imaging and photothermal destruction of malignancies (Huang et al., 2006; Sokolov et al., 2003). We

conjugated AuNPs to high-avidity ligands of three different membrane proteins of dorsal root ganglion (DRG) neurons and tested these conjugates for their ability to confer light-responsiveness to these cells. The investigated ligands included a synthetic molecule based on Ts1 neurotoxin from the venom of the Brazilian scorpion *Tityus serrulatus*, which binds voltage-gated sodium channels (Barhanin et al., 1982; Dang et al., 2014; Possani et al., 1977); antibodies targeting the TRPV1 ion channel; and antibodies targeting the $P2X_3$ receptor ion channel. The protein targets of all three of these ligands are known to be expressed in the membrane of DRG neurons (Hayes et al., 2000; Kostyuk et al., 1981; Xiang et al., 1998). We found that each of these AuNP conjugates binds to cultured DRG neurons and enables optical triggering of action potentials with remarkable robustness at low AuNP concentrations while displaying significant resistance to washout. By contrast, unconjugated AuNPs required higher concentration to allow for optical stimulation and washed away immediately upon solution exchange. The fact that this technique works well with all tested ligands suggests that this strategy is quite general. By appropriate selection of nanoparticle geometry, as well as choice of attached ligand, this conjugation technique should allow for selective stimulation of many excitable cell types with wavelengths ranging from the visible to NIR. With further development, nanoparticle-based direct photostimulation could provide an alternative to optogenetic techniques in situations where genetic manipulation is impractical.

Results

Non-functionalized AuNPs enable photo-excitation but wash out quickly

Our first experiment was to determine whether DRG neurons can be excited with visible light in the presence of 20 nm diameter AuNPs. DRG neurons were patch-clamped in the whole-cell configuration and transiently exposed to a 532 nm laser pulse (Figure 1A). AuNPs were added via perfusion through one side of a theta capillary, and they were washed away by perfusion of fresh buffer through the other side of the capillary (Figure 1B). Cells were stimulated with 300 pA of depolarizing current to produce a control action potential and verify cellular excitability; 200 ms subsequent to the electrically-stimulated action potential, a 174 mW laser pulse at 532 nm was delivered to the neuron for 1 ms. The laser was focused on the cell under study to produce an average irradiance of $\approx$31 kW/cm^2 (Figure S1). In the absence of AuNPs, no response to the laser flash was observed, either in the form of depolarization or membrane damage (Figure 1C). However, perfusion of 50 nM AuNPs onto the neurons rendered about 80% of tested cells (23 out of 29) sensitive to the laser pulse and an optically-induced action potential was produced. This effect depended strongly on the AuNP concentration near the cell, and active perfusion of fresh buffer rapidly washed the particles out, abolishing their effect. A second addition of 50 nM AuNPs restored light sensitivity. The time-course of the effect emphasizes that the non-functionalized AuNPs are removed from the cell surface within seconds of a perfusion wash (Figure 1D). Even without active washing, diffusion of AuNPs away from a cell is sufficient to abolish optical sensitivity within about two minutes (Figure S1).

Ts1-conjugated AuNPs are highly resistant to washing

We next attempted to induce AuNP localization to neuronal membranes by conjugating synthetic Ts1 to nanoparticles. Ts1, a neurotoxin that binds voltage-gated sodium channels without blocking them (Campos et al., 2007), was biotinylated and conjugated to streptavidin-coated AuNPs (Figure S2 and Supplemental Experimental Procedures). Upon application of this AuNP-Ts1 conjugate at 20 nM, a fraction of the cells tested (9 out of 21) became optically excitable with 1 ms laser pulses using powers as low as 126 mW, although 174 mW was a more reliable stimulus (Figures 2A,B). Significantly, many of these DRG neurons stayed sensitive to the laser pulse and fired action potentials for approximately 30 minutes under continuous perfusion wash (Figure 2C). The fact that the AuNP-Ts1 conjugate did not show equivalent activity in all tested cells, and that it worked in a significantly lower fraction of cells as compared to non-functionalized AuNPs ($P=0.016$, Fisher's exact test), is expected given the variable expression profiles of sodium channel types among different DRG neurons (see Discussion). Additionally, during these experiments, the neurons could be stimulated many times by the same 1 ms duration pulses of light without any indication of cell membrane damage or failure of the nanoparticle-cell linkage. These data suggest that the Ts1 promoted a close association of the AuNP with the neuronal membrane for the duration of the experiment. Importantly, under current clamp, the laser-induced membrane depolarization magnitude was proportional to laser power until the threshold potential was reached, at which point an action potential fired (Figure 2D). Furthermore, under voltage clamp, the membrane currents induced by the laser pulse were linearly modulated by laser power at a constant voltage (Figure S3). Similarly, at a constant laser power, DRG neurons treated with AuNP-Ts1 showed optically-induced currents with a linear dependence on membrane potential and a reversal potential near 0 mV (Figure S3). Together, these data show that the neurons are efficiently bound by the AuNP-Ts1 conjugate and that this link is well-behaved and stable over long periods.

One practical consideration with thermal stimulation methods is the risk of off-target or damaging effects from the temperature increase. Accordingly, minimizing temperature changes in a neuron's surrounding environment is likely advantageous as long as the neuron itself remains optically excitable. To investigate this, we measured the bath temperature ≈ 2 μm away from the stimulated neuron using a micropipette (see Experimental Procedures). As expected, when no nanoparticles were present, no increase in temperature was observed; when AuNP-Ts1 was bound to the neuron and an optically-induced action potential was present, a small temperature change was detected (Figure 2E). Importantly, strong binding of the nanoparticles to the target neuron allowed temperature changes in the cellular environment to be minimized. When 20 nM AuNP-Ts1 was initially present in the bath (similar to what is required with non-functionalized AuNPs), the temperature at the micropipette tip increased by more than 9°C in response to the laser flash (Figure 2F). After the excess AuNP-Ts1s were washed away, leaving only AuNP-Ts1s that were tightly attached to the neuron, the laser-induced elevation of temperature was only 1.5°C, representing more than an 80% decrease in temperature change (Figure 2F). This suggests that specific binding of AuNPs to target cells may allow for the safer use of nanoparticles with *in vivo* systems.

Functionalized AuNPs allow for repetitive stimulation without evidence of cellular damage

A question of central interest is whether there is an intrinsic limitation on the frequency of stimulation when using AuNPs, perhaps due to temperature buildup or some other effect. This issue is complicated by the fact that DRG neurons are a heterogeneous population with widely varying maximum firing frequencies; DRG somas have maximum firing frequencies from as low as 3 Hz to above 150 Hz depending on the DRG cell type (Waddell and Lawson, 1990). To explore this, we treated DRG neurons with AuNP-Ts1 and stimulated them with trains of laser pulses. In our studies, the maximum firing rate we were able to observe was 40 Hz. In this case, a series of 1 ms laser pulses delivered at 40 Hz for a total of 3 seconds stimulated an action potential with every stimulus, whereas a similar train at 50 Hz did not (Figure 3A). In other cells, we observed maximum firing frequencies as low as 15 Hz. An important distinction, then, is whether this maximum rate was limited by some property of the optical stimulus or whether we were simply observing the intrinsic maximum firing rate of the neuron. To address this, we compared a cell's maximum firing rate when stimulated optically versus when stimulated with an electrical current injection (Figure 3B). Optical and electrical stimuli of similar magnitudes (as measured by the rate of change of membrane potential during the respective stimuli) and equivalent 1 ms durations produced similar responses from the cell, as both trains stimulated action potential responses to about one third of the stimuli. We therefore conclude that in this case, the observed firing frequency was limited by the intrinsic properties of the neuron and is not a characteristic of stimulation with AuNPs. To corroborate this point, we tested the effect of the laser stimulus under voltage clamp at −100 mV (Figure 3C). At this membrane potential, neuronal channel activity is virtually eliminated and the laser-induced capacitive currents can be observed without confounding ion channel activity. We observed that the induced currents produced by laser pulses at 200 Hz are of similar magnitude to those produced by 40 Hz laser pulses and have no apparent abnormalities. This provides further evidence that the observed maximum action potential firing rate of 40 Hz is unrelated to the optical stimulation, and indicates that optical stimulus with AuNPs may be possible at much higher frequencies in other neuron types.

An important concern with this technique is whether stimulation mediated by AuNPs is harmful to a cell. While a single stimulus can kill a cell if excessive laser power is used (likely due to overheating), this does not seem to be a concern at lower power levels suitable for producing excitation. During this study of repetitive stimulation, some cells were optically stimulated to produce more than three thousand action potentials with no evidence of toxicity or cellular damage induced by the particles or the optical stimulation. Furthermore, over the course of these thousands of stimuli, there was no detected decrease in optical excitability. Cells that initially showed good responses to optical stimuli continued to fire action potentials in response to laser pulses until the patch seal failed. While these observations provide evidence against acute forms of toxicity at typical power levels, they do not rule out a chronic effect occurring over hours, days, months, or longer. Further investigations would need to be performed before AuNP stimulation is used for long-term studies.

AuNP-Ts1 allows optical stimulation of hippocampal brain slices and electrode-free investigation of activity

The above results, which demonstrate the utility of AuNPs for stimulating isolated DRG neurons in culture, led to the question whether similar AuNP-based optical stimulation is feasible in a complex neurological tissue. For this further test we employed an all optical method that avoided the need for electrodes of any kind. The experiments utilized acute slices of mouse hippocampus, a commonly-used *ex vivo* brain tissue preparation (Biscoe and Duchen, 1985). To provide optical stimulation, a small bolus of AuNP-Ts1 was injected into the CA1 region of the hippocampal slice (Figure 4A). Afterwards, the entire slice was perfused with the voltage-sensitive infrared dye indocyanine green (ICG) (Treger et al., 2014). We chose this dye because both its absorption and emission occur in the NIR spectrum and its fluorescence thus has excellent tissue penetration. For the experiment, ICG fluorescence was continuously monitored in the infrared while a short pulse of 532 nm light was delivered to the nanoparticles. A clear, transient reduction in ICG fluorescence can be seen in response to a 225 mW, 10 ms optical stimulus (Figure 4B). As ICG shows a decreasing fluorescence with increasing membrane potential, this signal implies cellular depolarization, as expected. The brain slices required a significantly stronger optical stimulus compared to cultured DRG neurons. This is likely due to the fact that the spot size of the 532 nm laser was much larger in the brain slice setup (due to a lower numerical aperture objective and scattering in the tissue), thus reducing the power density of the spot. In addition to simple depolarization, paired pulse facilitation was observed in response to closely-spaced stimuli (Figure S4). Finally, this technique allows for spatial maps of neural activity to be constructed. Figure 4C shows a visual time course of neural activity. Immediately following the stimulus, significant depolarization predominates in the region of observation. Over time, this evolves toward a mixture of small, localized regions of depolarization and hyperpolarization that average out to the baseline level of activity. These data show that combining AuNPs with a voltage-sensitive dye such as ICG can allow for neurological studies in complex tissues without the physical restrictions associated with electrodes.

Antibodies can be used to bind AuNPs to target cells

Although Ts1 proved capable of binding AuNPs to DRG neurons, we next pursued a more general strategy for linking AuNPs to a target of interest by using antibodies as the AuNP-anchoring molecules. For the case of DRG neurons, we chose TRPV1 and the $P2X_3$ receptor as antibody targets since these proteins are more highly expressed in neurons than in glia. Antibodies to these two targets (TRPV1ab and $P2X_3$ab, respectively) were chemically biotinylated (see Supplemental Experimental Procedures) and incubated with DRG cells overnight. After multiple buffer exchanges the next day, recording began. As expected, the neurons were insensitive to light before streptavidin-functionalized AuNPs (AuNP-SAs) were present, whereas exposure to AuNP-SAs rapidly sensitized both TRPV1ab- and $P2X_3$ab-labeled cells to 126 mW, 1 ms optical stimuli (Figure 5A,B). As with AuNP-Ts1, not all neurons treated with AuNP-SAs became sensitive to optical stimuli (11 out of 19), likely due to variable expression of the target membrane proteins (see Discussion). Antibody-labeled neurons which became sensitized to laser pulses retained this sensitivity

for more than 20 minutes under continuous convective washing (Figure 5C,D). Thus, the AuNPs were tightly linked to DRG cells by the antibodies.

Despite the workability of the biotinylated antibodies as AuNP-anchoring molecules, they require either chemical biotinylation of primary antibodies, or the purchase of biotinylated primary antibodies which must often be custom-ordered at higher cost. Since it is often more convenient to use unmodified primary antibodies, we investigated the alternative AuNP binding strategy of using AuNPs functionalized with secondary antibodies (AuNP-2ab). We first incubated DRG neurons overnight with unmodified TRPV1ab or $P2X_3$ab antibodies. As before, we washed the cells extensively the next day prior to recording. Once again, no optical excitability was detected before application of the nanoparticles (Figure 6A,B). Addition of AuNP-2abs to the cells quickly conferred sensitivity to the 126 mW, 1 ms laser pulses to a fraction of the tested cells (9 out of 15), and this photosensitivity remained resistant to washout (Figure 6C,D). AuNP-2abs bound to unmodified primary antibodies performed similarly to AuNP-SAs bound to biotinylated primary antibodies in terms of ability to sensitize neurons to light. In future applications, the choice of which to use would likely depend on convenience for, or specific requirements of, the intended application.

A third labeling strategy attempted with the antibodies was to pre-mix biotinylated TRPV1ab or biotinylated $P2X_3$ab with AuNP-SA to produce AuNP-antibody conjugates (AuNP-TRPV1ab and AuNP-$P2X_3$ab); we then applied these pre-formed conjugates to the neurons. Both AuNP-TRPV1ab and AuNP-$P2X_3$ab at concentrations of 20 nM rendered neurons light-sensitive (Figures S4 and S5). Furthermore, both AuNP-TRPV1ab and AuNP-$P2X_3$ab were highly efficient; only 48 mW of light delivered to the neuron for 1 ms was sufficient to reliably produce action potentials with these pre-formed conjugates, whereas this power was never sufficient to trigger action potentials using the other AuNP preparations. However, presumably as a consequence of this high efficiency of light energy collection, the AuNP-antibody (AuNP-ab) conjugates mediated thermal damage of the neurons, likely because they formed large clusters (see Discussion). Following a laser pulse, an abnormal and persistent membrane depolarization indicating cell damage was frequently observed following the action potential, along with loss of excitability. In most cases, the resting potential spontaneously recovered and excitability returned after several seconds (Figures S5 and S6). Although the improved optical sensitivity of the neurons might be advantageous for some applications, the increased propensity for cellular damage may well be limiting in other circumstances.

AuNP-based optical excitability is due to heat-induced changes in membrane capacitance

A mechanism has been described whereby a rapidly-delivered pulse of heat directly depolarizes cell membranes by transiently changing their capacitances (Shapiro et al., 2012), which was the basis of our working hypothesis when using AuNPs. As noted above, AuNPs absorb 532 nm light and convert this energy into heat. Accordingly, we hypothesized that the light-sensitivity in cells treated with AuNPs is intrinsically related to the membrane and does not involve temperature sensitivity of any membrane proteins. To investigate this mechanism, we tested the effects of AuNP treatment on light-induced electrophysiological properties of horizontal planar membranes composed of asolectin. Under voltage clamp, and

following delivery of AuNPs to the upper surface of the bilayer, laser pulses as short as 0.1 ms induced currents that were similar to those produced in the neurons. The current amplitudes did not increase linearly with pulse duration; rather, they reached a saturating value with 0.5 ms and longer laser pulses (Figure 7A). These currents were negative at negative voltages, changed polarity when the voltage was close to 0 mV, and were positive at positive voltages with a linear current-voltage relationship (Figure 7B). In addition to the linear dependence on membrane potential, the current response also varied roughly linearly with laser power (Figure 7C). Temperatures measured near the membrane behaved similarly to capacitance in that they transiently rose in response to a laser pulse before slowly returning to baseline (Figure 7D). However, the measured temperatures continued to rise for several milliseconds following the end of a laser pulse, which was interesting and unexpected. Capacitances of the membranes were measured by applying a sinusoidal voltage to the system and calculating the resulting impedance (Supplemental Experimental Procedures). We found that the capacitance rapidly increased during a laser pulse and decreased much more slowly after the pulse was turned off (Figure 7E). The time constant of the decrease in capacitance following the end of a laser pulse was 10.2 ms with a 1 ms laser pulse (Figure 7F), considerably faster than was observed with direct IR heating (Shapiro et al., 2012), but still slow enough that it did not produce a significant dC/dt, which is necessary to induce a capacitive current. The dynamics of capacitance change largely reflected the observed temperature changes in the system, and both behaved somewhat nonlinearly with respect to pulse duration.

To help us understand this counterintuitive observation, as well as interpret our broader results in the context of the hypothesized mechanism, we mathematically modeled a system of membrane-associated gold nanoparticles in response to incident laser pulses. The diffusion of heat from the nanoparticles to the membrane was solved for different nanoparticle geometries, and the effects of the resulting temperature changes were calculated (Figure S7, Supplemental Experimental Procedures). The results from the model were broadly in line with our experimental results and clarified some features of the system. For example, the above-noted continued rise in temperature after the end of the laser pulse appears to reflect the inability to place the temperature-measuring micropipette as close to the bilayer as is possible with DRG neurons, due to the geometry and optics of the bilayer system. This increased distance from the membrane caused a time-lag in our observations as heat from the AuNPs required several milliseconds to diffuse to our measurement location (Figure S8). This lag also manifested as a slowed onset of temperature increase following a laser pulse; as expected, this delay was not present in the capacitance measurements, as those were recorded directly in the lipid membrane. An additional benefit of the model is that it allows a rough calculation of the amount of capacitive current generated by a single nanoparticle in response to a given laser pulse. Based on our calculations of the number of particles adhered to a DRG neuron combined with the total current produced by the particles, we find that a single particle under an irradiance of 18 kW/cm^2 produces approximately 0.75 pA of current. The depolarization produced by such a current will depend on the membrane capacitance of the cell under consideration.

Discussion

In this work, we first showed that neurons can be stimulated with visible light in the presence of 20 nm spherical AuNPs. This was expected as neuronal stimulation has been previously shown with NIR wavelengths (Eom et al., 2014; Yong et al., 2014). While visible light has poorer tissue penetrance than NIR light (Bashkatov et al., 2005), it may be advantageous in applications such as vision restoration in diseased retina (see below). Importantly, the present experiments also demonstrate certain shortcomings of unmodified AuNPs for optical excitation. In particular, they must be present at relatively high concentrations to be effective, and they are easily washed away from the target neurons in a few seconds with convective solution exchange.

To overcome these limitations, we employed a strategy of conjugating the AuNPs to molecules which bind neuronal membrane proteins with high avidity as a strategy to place the AuNPs close to the neuronal membrane and avoid diffusion of the nanoparticles away from the neuron. These molecules included the scorpion toxin Ts1 which targets voltage-gated sodium channels, and antibodies that target TRPV1 and $P2X_3$ ion channels expressed by DRG neurons. Remarkably, all of these ligands substantially facilitated binding of the AuNPs to the target neurons without impeding their excitatory capability. It is important to note that all three ligands tested showed activity in only a fraction of cells (29 out of 55, pooled together), whereas non-functionalized AuNPs worked in the large majority of cells (23 out of 29). This difference is statistically significant at α=0.05 (P=0.0195, Fisher's exact test), and is expected because DRG neurons are a highly diverse collection of cells representing the majority of somatosensory phenotypes in the body (Omri and Meiri, 1990). Cells of different sensory specialization can express very different profiles of membrane receptors, a fact which motivated this study and our approach to cell targeting. For example, TRPV1 is classically associated with thermosensitive neurons, while $P2X_3$ receptors are usually associated with nociceptive neurons (Burnstock, 2000; Greffrath et al., 2003). Neurons of different phenotypes thus can exhibit markedly different levels of expression of these channels; in cells with low expression, AuNP binding would likely be insufficient to produce optical sensitivity with the laser powers used in this study. In contrast, non-functionalized nanoparticles were used at high concentration and without washing them out, allowing them to stimulate most excitable cells regardless of their expression profiles. Although ligand-functionalized nanoparticles did not readily attach to all neurons, when the nanoparticles did bind to a cell they were highly resistant to washout. Neurons treated with AuNP-Ts1 remained optically sensitized after more than 30 minutes of continuous convective solution exchange, and antibody-conjugated nanoparticles performed similarly. Importantly, even when AuNPs are bound to membrane ion channels such as TRPV1, their effect is independent of the activity of the channel. Specifically, they depolarize the membrane by directly changing membrane capacitance rather than by opening the ion channels to which they are ligated. This allows for much faster depolarization than in other strategies where nanoparticle heating leads to opening of temperature-sensitive ion channels (Stanley et al., 2012). The rapid depolarization enabled by the present technique involving membrane capacitance change is critical for temporally precise stimulation of neuronal activity. Finally, tight binding of nanoparticles to the target neuron allowed for minimization

of off-target environmental heating once excess particles were removed. These properties are likely to be of significant benefit *in vivo*, where concentrations of exogenous molecules must be limited to avoid toxicity and where interstitial fluids are constantly being circulated. Additionally, given that all of the investigated molecules conjugated with AuNPs enabled robust photostimulation, it is likely that other AuNP-anchoring biological ligands can be used to preferentially target different classes of excitable cells. Although this work exclusively utilized 20 nm spherical gold nanoparticles with their associated absorption peak at 523 nm, this excitation regime may not be ideal for all purposes. For instance, stimulation with NIR light around 800 nm may be optimal for many *in vivo* applications due to its high tissue penetrance and much lower absorption by hemoglobin as compared to 532 nm light. Fortunately, a variety of different sizes and shapes of nanoparticles are commercially available, possessing plasmon band absorption peaks ranging from around 500 nm to more than 2 μm. The chemical functionalizations described here should be readily applicable to this array of nanoparticles, allowing optical stimulation with the wavelength best-suited to a specific application.

A particularly interesting phenomenon observed in these experiments is that the efficiency of photostimulation with AuNP-antibody conjugates exhibits a striking dependence on the labeling method. When the AuNP-streptavidin is mixed with biotinylated antibodies prior to incubation with neurons, the cells are much more strongly excited (often to the point of damage) than when the neurons are incubated with primary antibodies, washed with buffer, and then incubated with the functionalized AuNPs. The likely cause of both the improved excitation efficiency and the increased propensity for damage with the pre-mixed AuNP-antibodies is the formation of large AuNP clusters. In the case of AuNP-Ts1, a single toxin molecule can bind only one AuNP, so multiple nanoparticles cannot link together. In contrast, the biotinylation process likely attaches multiple biotin molecules at various sites to each antibody (Supplemental Experimental Procedures), while the nanoparticles have an average of nine streptavidin molecules per AuNP. This presumably allows for the formation of arbitrarily large branching complexes via multiple streptavidin-biotin reactions. Thus, a single reaction linking an antibody to its epitope on a neuron could potentially adhere many cross-linked nanoparticles to the neuron at a single location. Conversely, when the biotinylated antibodies and nanoparticles are applied sequentially, they cannot form clusters since they are not present in solution at the same time. The presence of large clusters is expected to greatly increase the number of AuNPs bound to a given neuron, thus increasing the heat generated in the cell's immediate environment by a given incident optical power. While the increased tendency for cellular damage associated with these cross-linked AuNP structures makes their use questionable for neuronal stimulation, they may find utility in applications such as targeted cell ablation or cancer photothermal therapy where induction of cell death is the objective (Kennedy et al., 2011).

Our results obtained with planar lipid bilayers revealed that laser-induced heating of a lipid bilayer produces changes in bilayer capacitance. These changes drive currents which, in a cellular environment, would alter the transmembrane potential. This process occurred in the absence of any membrane proteins, indicating that ion channels and other membrane proteins are not necessary for the mechanism of neuronal stimulation via AuNPs. As

expected when we conceived these experiments, this process is qualitatively similar to the method of direct heating with an IR laser (Shapiro et al., 2012). However, the cooling kinetics observed here after a laser pulse are faster by an order of magnitude or more. This disparity can be explained by the fact that the IR laser pulse is absorbed by a relatively large solution volume; the large excitation volume generates a large amount of heat, and dissipation of this heat requires a relatively long diffusion distance. AuNPs, by contrast, heat only their immediate environment, and the smaller total heat generation results in a shortened diffusion path length for cooling. Importantly, these experiments demonstrated that the size of the depolarizing current depends on the rate of change of temperature (i.e. the derivative), not on the temperature itself. This means that sizeable depolarizations can be obtained without raising the temperature to damaging levels by heating a cell quickly while keeping the duration of heating very short.

The present approach, employing a cell-targeting anchor to intimately localize the AuNP photosensor at the membrane for photothermal cell activation, represents a potentially widely applicable advance in the technology of neuronal optical stimulation. This work has potential applications in at least two distinct fields. First, it could be used as an alternative to optogenetics in fundamental research. Functionalized AuNPs allow for high-avidity binding and stimulation of neurons without damaging the cells. Furthermore, nanoparticles present potential advantages versus optogenetics. The use of functionalized AuNPs does not require transfection or genetic modification of the organisms or tissues of interest. This makes the AuNP technique particularly suitable for use in species where genetic manipulation is less well-developed or where the cells/tissue/organism under study cannot survive over an extended transfection period. As in the cases of pharmacological approaches for establishing light-sensitivity of native, unmodified ion channels (Lester et al., 1980; Mourot et al., 2013; Yue et al., 2012), the period required for inducing light sensitivity with cell-targeted AuNP conjugates is essentially that needed for access of the administered conjugates to the cells (for *in vitro* preparations as in the present study, as little as several minutes). Despite these advantages, nanoparticles also have important limitations compared to optogenetics. In addition to stimulation, optogenetics can provide neuronal inhibition and optical readouts of neuronal activity via expression of molecules such as halorhodopsins and voltage-sensitive fluorescent proteins (Akemann et al., 2012; Zhang et al., 2007). Nanoparticles, to our knowledge, are strictly limited to stimulation as inhibition would require an optically-induced cooling effect, which seems unlikely. Furthermore, unlike the essentially permanent expression of light-sensitive proteins induced by optogenetic modification of cells, the clearance and/or degradation of delivered AuNP conjugates likely limit the lifetime of cell photosensitivity induced by AuNP treatment; thus, for long-term study, AuNP-based methods would likely require repeat treatment. Another potential limitation of nanoparticles is their broad (and in the case of non-spherical particles, multiple) peaks of plasmon absorption. This may limit the ability to independently excite multiple cell types using different wavelengths, a technique that is possible with optogenetics (Prigge et al., 2012).

A second field of possible application of AuNP-enabled neuronal photostimulation is that of human therapeutics. One therapeutic goal that may be addressable via AuNP treatment is the enabling of direct photostimulation of retinal ganglion cells (RGCs) in patients who suffer

from photoreceptor degenerative diseases, such as age-related macular degeneration or retinitis pigmentosa. RGCs are “retinal output” neurons that, in the healthy retina, transmit action potentials to the brain which encode visual signals initiated by the retina’s rod and cone photoreceptors. There is ample evidence that, in many instances of advanced-stage photoreceptor degenerative diseases, RGCs remain healthy despite the deterioration and loss of the native rods and cones (Margolis et al., 2008; Mazzoni et al., 2008; Medeiros and Curcio, 2001). In this situation, functionalized AuNPs similar to those used in the present study could be injected into the eye where they would bind to the RGCs, allowing light entering the eye to directly excite the RGCs and thus bypass the inoperative photoreceptors. The critical importance of achieving vision repair in photoreceptor degenerative diseases is motivating approaches that currently include opto-electronic, optogenetic, pharmacological, and other strategies to engineer light sensitivity of RGCs or other retinal neurons (Bharti et al., 2014; Bi et al., 2006; Caporale et al., 2011; Chader et al., 2009; Greenberg et al., 2011; Lagali et al., 2008; Polosukhina et al., 2012; Theogarajan, 2012). The present experimental findings with conjugated AuNPs open a new avenue that may benefit progress toward this important objective.

Experimental Procedures

DRG cells were cultured from neonatal rats and used 1 to 7 days thereafter (see supplemental experimental procedures for more details on this and all other procedures). For experiments where antibodies were used to link AuNPs to neurons, the primary antibodies (TRPV1ab and $P2X_3$ab) were added to the neuron cell culture medium and kept overnight in the incubator. Experiments were performed the next day, and AuNP-SA or AuNP-2ab was added during the experiment as shown in the data. For DRG neurons under current clamp, current injections were always 1 ms in duration and varied in amplitude from 300 pA to 700 pA based on what level was necessary to produce robust stimulation in a given cell. Similarly, laser pulses in DRG neurons were also always 1 ms in duration and power was varied as described in our results. All DRG experiments were performed using a 40X microscope objective lens to focus the laser onto the cells. Hippocampal slices were harvested from adult mice and immediately stored in artificial cerebrospinal fluid (aCSF) bubbled with carbogen. Immediately before use, a slice was injected with a mixture of 20 nM AuNP-Ts1 and a fluorescent dye (to allow the injection site to be visualized). The slices were then immersed in a perfusion chamber and stained with ICG dissolved in aCSF for 5 minutes. Finally, perfusion of carbogen-bubbled aCSF was turned on to clear away excess ICG and keep the tissue oxygenated. ICG was imaged using 780 nm excitation through a 20X objective in epifluorescence configuration through the glass floor of the perfusion chamber. Optical stimulation was performed through a 32X objective mounted above the prep. Planar lipid bilayers were formed from asolectin in a horizontal hole 300 μm in diameter. Due to the geometry of the bilayer chamber, we were unable to use the same microscope objective as with the DRG neurons. Instead, a 10X objective was used. This results in a lower degree of focusing of the laser, and thus laser powers are not directly comparable between the two systems. Temperatures were measured by monitoring changes in resistance of calibrated micropipettes (Yao et al., 2009). Capacitances of planar bilayers were monitored by applying sinusoidal command voltages and observing the resulting

sinusoidal currents. The impedance of the system is largely determined by the capacitance of the bilayer for high-frequency inputs. The command signal used in this work had a frequency of 5 kHz. Data analysis, mathematical modeling, and chemical syntheses are described in detail in the supplemental experimental procedures. All animal protocols used in this work were approved by the University of Chicago Animal Care and Use Committee.

Supplementary Material

Refer to Web version on PubMed Central for supplementary material.

Acknowledgments

We thank Dr. Karol S. Bruzik, Dr. Pavel Y. Savechenkov and Dr. Christoph H. Grein (Univ. of Illinois at Chicago), Dr. Lan Yue (Univ. of Southern California), and Dr. Tijana Rajh (Argonne National Laboratory) for helpful discussions during the course of this study. We are especially indebted to Dr. Deborah Nelson and Dr. Vladimir Riazanski (University of Chicago) for their assistance in harvesting brain slices and guidance on their use. Supported by NIH grants EY023430, GM030376 and EY001792; the Beckman Initiative for Macular Research (Los Angeles, CA); and Research to Prevent Blindness, (New York, NY).

References

Akemann W, Mutoh H, Perron A, Park YK, Iwamoto Y, Knöpfel T. Imaging neural circuit dynamics with a voltage-sensitive fluorescent protein. J Neurophysiol. 2012; 108:2323–2337. [PubMed: 22815406]

Allègre G, Avrillier S, Albe-Fessard D. Stimulation in the rat of a nerve fiber bundle by a short UV pulse from an excimer laser. Neurosci Lett. 1994; 180:261–264. [PubMed: 7700591]

Barhanin J, Giglio JR, Léopold P, Schmid A, Sampaio SV, Lazdunski M. Tityus serrulatus venom contains two classes of toxins. Tityus gamma toxin is a new tool with a very high affinity for studying the Na+ channel. J Biol Chem. 1982; 257:12553–12558. [PubMed: 6290472]

Bashkatov AN, Genina EA, Kochubey VI, Tuchin VV. Optical properties of human skin, subcutaneous and mucous tissues in the wavelength range from 400 to 2000 nm. J Phys Appl Phys. 2005; 38:2543.

Bharti K, Rao M, Hull SC, Stroncek D, Brooks BP, Feigal E, van Meurs JC, Huang CA, Miller SS. Developing cellular therapies for retinal degenerative diseases. Invest Ophthalmol Vis Sci. 2014; 55:1191–1202. [PubMed: 24573369]

Bi A, Cui J, Ma YP, Olshevskaya E, Pu M, Dizhoor AM, Pan ZH. Ectopic expression of a microbial-type rhodopsin restores visual responses in mice with photoreceptor degeneration. Neuron. 2006; 50:23–33. [PubMed: 16600853]

Biscoe TJ, Duchen MR. An Intracellular Study of Dentate, Ca1 and Ca3 Neurones in the Mouse Hippocampal Slice. Q J Exp Physiol. 1985; 70:189–202. [PubMed: 4011835]

Burnstock G. P2X receptors in sensory neurones. Br J Anaesth. 2000; 84:476–488. [PubMed: 10823099]

Campos FV, Chanda B, Beirão PSL, Bezanilla F. β-Scorpion Toxin Modifies Gating Transitions in All Four Voltage Sensors of the Sodium Channel. J Gen Physiol. 2007; 130:257–268. [PubMed: 17698594]

Caporale N, Kolstad KD, Lee T, Tochitsky I, Dalkara D, Trauner D, Kramer R, Dan Y, Isacoff EY, Flannery JG. LiGluR restores visual responses in rodent models of inherited blindness. Mol Ther J Am Soc Gene Ther. 2011; 19:1212–1219.

Chader GJ, Weiland J, Humayun MS. Artificial vision: needs, functioning, and testing of a retinal electronic prosthesis. Prog Brain Res. 2009; 175:317–332. [PubMed: 19660665]

Dang B, Kubota T, Correa AM, Bezanilla F, Kent SBH. Total Chemical Synthesis of Biologically Active Fluorescent Dye-Labeled Ts1 Toxin. Angew Chem. 2014; 126:9116–9120.

Eom K, Kim J, Choi JM, Kang T, Chang JW, Byun KM, Jun SB, Kim SJ. Enhanced Infrared Neural Stimulation using Localized Surface Plasmon Resonance of Gold Nanorods. Small Weinh Bergstr Ger. 2014

Ginn SL, Alexander IE, Edelstein ML, Abedi MR, Wixon J. Gene therapy clinical trials worldwide to 2012 - an update: Gene therapy clinical trials worldwide to 2012 - an update. J Gene Med. 2013; 15:65–77. [PubMed: 23355455]

Greenberg KP, Pham A, Werblin FS. Differential targeting of optical neuromodulators to ganglion cell soma and dendrites allows dynamic control of center-surround antagonism. Neuron. 2011; 69:713–720. [PubMed: 21338881]

Greffrath W, Binzen U1, Schwarz ST, Saaler-Reinhardt S, Treede RDC. Co-expression of heat sensitive vanilloid receptor subtypes in rat dorsal root ganglion neurons. [Miscellaneous Article]. Neuroreport. 2003 Dec 2.14:2251–2255. [PubMed: 14625457]

Hayes P, Meadows HJ, Gunthorpe MJ, Harries MH, Duckworth DM, Cairns W, Harrison DC, Clarke CE, Ellington K, Prinjha RK, et al. Cloning and functional expression of a human orthologue of rat vanilloid receptor-1. Pain. 2000; 88:205–215. [PubMed: 11050376]

Hirase H, Nikolenko V, Goldberg JH, Yuste R. Multiphoton stimulation of neurons. J Neurobiol. 2002; 51:237–247. [PubMed: 11984845]

Huang X, El-Sayed IH, Qian W, El-Sayed MA. Cancer Cell Imaging and Photothermal Therapy in the Near-Infrared Region by Using Gold Nanorods. J Am Chem Soc. 2006; 128:2115–2120. [PubMed: 16464114]

Kennedy LC, Bickford LR, Lewinski NA, Coughlin AJ, Hu Y, Day ES, West JL, Drezek RA. A New Era for Cancer Treatment: Gold-Nanoparticle-Mediated Thermal Therapies. Small. 2011; 7:169–183. [PubMed: 21213377]

Kostyuk PG, Veselovsky NS, Tsyndrenko AY. Ionic currents in the somatic membrane of rat dorsal root ganglion neurons-I. Sodium currents. Neuroscience. 1981; 6:2423–2430. [PubMed: 6275294]

Lagali PS, Balya D, Awatramani GB, Münch TA, Kim DS, Busskamp V, Cepko CL, Roska B. Light-activated channels targeted to ON bipolar cells restore visual function in retinal degeneration. Nat Neurosci. 2008; 11:667–675. [PubMed: 18432197]

Lester HA, Krouse ME, Nass MM, Wassermann NH, Erlanger BF. A covalently bound photoisomerizable agonist: comparison with reversibly bound agonists at Electrophorus electroplaques. J Gen Physiol. 1980; 75:207–232. [PubMed: 6246192]

Lugo K, Miao X, Rieke F, Lin LY. Remote switching of cellular activity and cell signaling using light in conjunction with quantum dots. Biomed Opt Express. 2012; 3:447–454. [PubMed: 22435093]

Margolis DJ, Newkirk G, Euler T, Detwiler PB. Functional stability of retinal ganglion cells after degeneration-induced changes in synaptic input. J Neurosci Off J Soc Neurosci. 2008; 28:6526–6536.

Mazzoni F, Novelli E, Strettoi E. Retinal ganglion cells survive and maintain normal dendritic morphology in a mouse model of inherited photoreceptor degeneration. J Neurosci Off J Soc Neurosci. 2008; 28:14282–14292.

Medeiros NE, Curcio CA. Preservation of ganglion cell layer neurons in age-related macular degeneration. Invest Ophthalmol Vis Sci. 2001; 42:795–803. [PubMed: 11222543]

Mourot A, Tochitsky I, Kramer RH. Light at the end of the channel: optical manipulation of intrinsic neuronal excitability with chemical photoswitches. Front Mol Neurosci. 2013; 6:5. [PubMed: 23518818]

Omri G, Meiri H. Characterization of sodium currents in mammalian sensory neurons cultured in serum-free defined medium with and without nerve growth factor. J Membr Biol. 1990; 115:13–29. [PubMed: 2159518]

Packer AM, Roska B, Häusser M. Targeting neurons and photons for optogenetics. Nat Neurosci. 2013; 16:805–815. [PubMed: 23799473]

Polosukhina A, Litt J, Tochitsky I, Nemargut J, Sychev Y, De Kouchkovsky I, Huang T, Borges K, Trauner D, Van Gelder RN, et al. Photochemical restoration of visual responses in blind mice. Neuron. 2012; 75:271–282. [PubMed: 22841312]

Possani LD, Alagón AC, Fletcher PL Jr, Erickson BW. Purification and properties of mammalian toxins from the venom of the Brazilian scorpion Tityus serrulatus Lutz and Mello. Arch Biochem Biophys. 1977; 180:394–403. [PubMed: 879793]

Prigge M, Schneider F, Tsunoda SP, Shilyansky C, Wietek J, Deisseroth K, Hegemann P. Color-tuned Channelrhodopsins for Multiwavelength Optogenetics. J Biol Chem. 2012; 287:31804–31812. [PubMed: 22843694]

Roper DK, Ahn W, Hoepfner M. Microscale Heat Transfer Transduced by Surface Plasmon Resonant Gold Nanoparticles. J Phys Chem C. 2007; 111:3636–3641.

Shapiro MG, Homma K, Villarreal S, Richter CP, Bezanilla F. Infrared light excites cells by changing their electrical capacitance. Nat Commun. 2012; 3:736. [PubMed: 22415827]

Sokolov K, Follen M, Aaron J, Pavlova I, Malpica A, Lotan R, Richards-Kortum R. Real-Time Vital Optical Imaging of Precancer Using Anti-Epidermal Growth Factor Receptor Antibodies Conjugated to Gold Nanoparticles. Cancer Res. 2003; 63:1999–2004. [PubMed: 12727808]

Stanley SA, Gagner JE, Damanpour S, Yoshida M, Dordick JS, Friedman JM. Radio-Wave Heating of Iron Oxide Nanoparticles Can Regulate Plasma Glucose in Mice. Science. 2012; 336:604–608. [PubMed: 22556257]

Theogarajan L. Strategies for restoring vision to the blind: current and emerging technologies. Neurosci Lett. 2012; 519:129–133. [PubMed: 22414860]

Treger JS, Priest MF, Iezzi R, Bezanilla F. Real-Time Imaging of Electrical Signals with an Infrared FDA-Approved Dye. Biophys J. 2014; 107:L09–L12. [PubMed: 25229155]

Waddell PJ, Lawson SN. Electrophysiological properties of subpopulations of rat dorsal root ganglion neurons in vitro. Neuroscience. 1990; 36:811–822. [PubMed: 2234413]

Wells J, Kao C, Mariappan K, Albea J, Jansen ED, Konrad P, Mahadevan-Jansen A. Optical stimulation of neural tissue in vivo. Opt Lett. 2005; 30:504–506. [PubMed: 15789717]

Xiang Z, Bo X, Burnstock G. Localization of ATP-gated P2X receptor immunoreactivity in rat sensory and sympathetic ganglia. Neurosci Lett. 1998; 256:105–108. [PubMed: 9853714]

Yao J, Liu B, Qin F. Rapid Temperature Jump by Infrared Diode Laser Irradiation for Patch-Clamp Studies. Biophys J. 2009; 96:3611–3619. [PubMed: 19413966]

Yong J, Needham K, Brown WGA, Nayagam BA, McArthur SL, Yu A, Stoddart PR. Gold-Nanorod-Assisted Near-Infrared Stimulation of Primary Auditory Neurons. Adv Healthc Mater. 2014

Yue L, Pawlowski M, Dellal SS, Xie A, Feng F, Otis TS, Bruzik KS, Qian H, Pepperberg DR. Robust photoregulation of GABA(A) receptors by allosteric modulation with a propofol analogue. Nat Commun. 2012; 3:1095. [PubMed: 23033071]

Zhang F, Wang LP, Boyden ES, Deisseroth K. Channelrhodopsin-2 and optical control of excitable cells. Nat Methods. 2006; 3:785–792. [PubMed: 16990810]

Zhang F, Wang LP, Brauner M, Liewald JF, Kay K, Watzke N, Wood PG, Bamberg E, Nagel G, Gottschalk A, et al. Multimodal fast optical interrogation of neural circuitry. Nature. 2007; 446:633–639. [PubMed: 17410168]

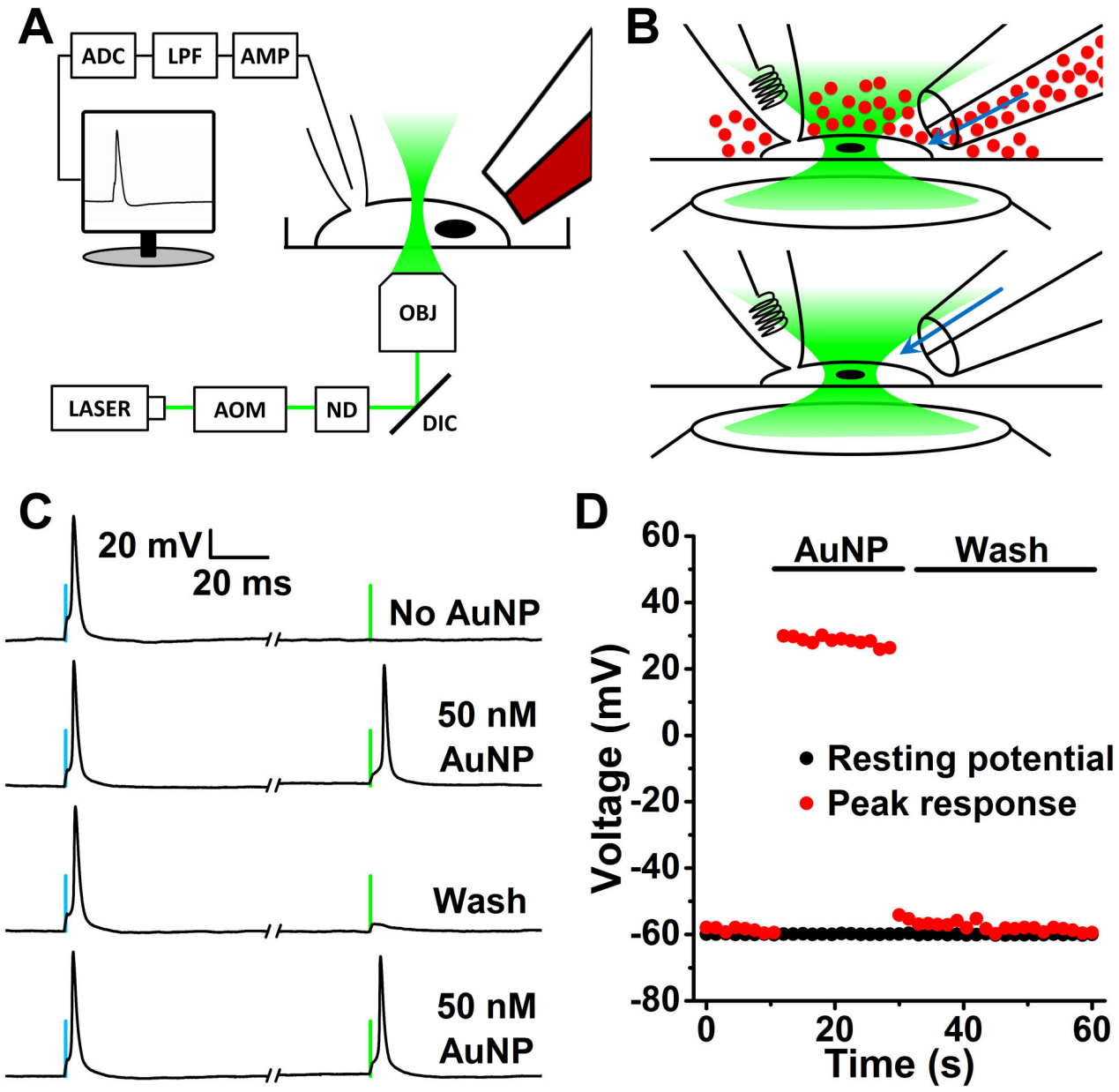

Figure 1.

Action potentials can be stimulated by 532 nm light using AuNPs. (A) Diagram of the experimental setup. The cell is patch-clamped in a whole-cell configuration (pipette on the left), and both AuNP addition and perfusion washing are accomplished via the theta capillary on the right. Abbreviations are as follows: AOM – acousto-optic modulator, ND – neutral density filters, DIC – dichroic mirror, OBJ – microscope objective, AMP – amplifier, LPF – low-pass filter, ADC – analog-to-digital converter. Many parts of the diagram are not drawn to scale. (B) AuNPs were perfused over a patch-clamped DRG neuron through one side of a theta capillary. After a sufficient optical response is observed, fresh buffer is perfused over the cell from the other side of the capillary, washing away the AuNPs. (C) Representative traces of current-clamped DRG cells firing action potentials in response to

two different stimuli: a 300 pA, 1 ms current injection (left side, blue bars) and a 174 mW, 1 ms 532 nm laser pulse (right side, green bars). Initially, cells were responsive only to the electrical stimulus, but a bolus of AuNPs sensitized the cells to light. Washing removed enough AuNPs from the cell that the laser effect became insufficient to trigger an action potential. Optical excitability returned when a second bolus was added to the bath. (D) An active washing system demonstrates how the laser effect is dependent on AuNP concentration near the cell. Upon washing, the laser effect rapidly disappears within seconds. “Peak response” is the maximum voltage reached following a laser pulse. See also Figure S1.

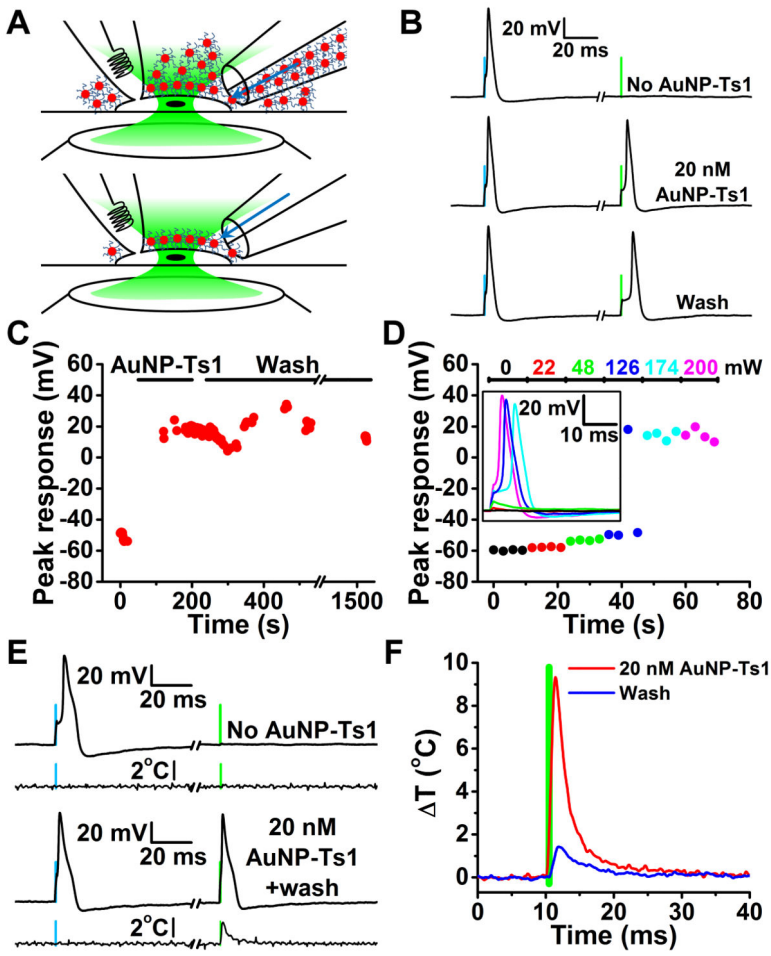

Figure 2.

Optical stimulation of DRG neurons with AuNP-Ts1. (A) A procedure identical to that used with non-functionalized AuNPs (Figure 1B) is unable to wash AuNP-Ts1 from the cell. (B) As with non-functionalized AuNPs, DRG neurons initially respond only to electrical stimuli (500 pA, 1 ms – blue bars), but addition of AuNP-Ts1 sensitizes them to optical stimuli (174 mW, 532 nm, 1ms – green bars). Here, however, washing does not quickly eliminate optical excitability. (C) Even after 20 minutes of continuous washing, neurons labeled with AuNP-Ts1 remain optically excitable. (D) Increasing laser power causes increasing cell depolarizations, triggering action potentials once the cell's threshold voltage is reached. 174 mW is necessary to reliably stimulate this particular neuron. (Inset) Sample traces for each laser power. (E) In the absence of AuNP-Ts1 (top two traces), no temperature changes were observed 2 μm away from a DRG cell during either electrical (blue bar) or optical (green bar) stimulation. After adding AuNP-Ts1 and washing away excess nanoparticles (bottom two traces), an increase in temperature was measured during optical stimulation. Temperature traces are single recordings with noise subtraction and are filtered at 1 kHz. (F) With nanoparticles present in the bulk solution (before washing), a large change in temperature is observed. Active perfusion washing leaves only the nanoparticles tightly bound to the surface. The cell remains optically excitable, but the temperature change

measured 2 μm from the cell decreases dramatically. Green bar shows the optical stimulus. Traces are averages of 20 recordings and are filtered at 1 kHz. See also Figures S2 and S3.

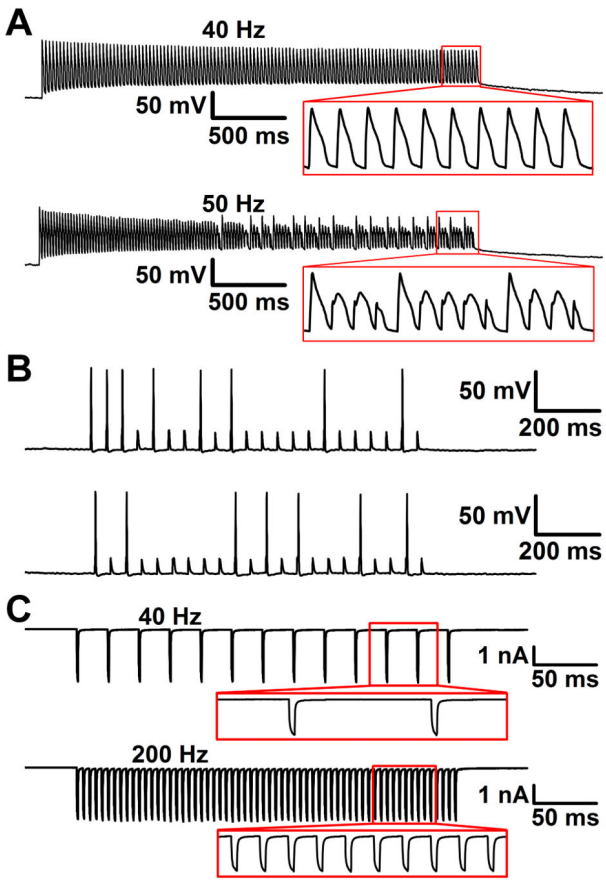

Figure 3.

AuNPs are able to stimulate action potentials at a rate of at least 40 Hz. (A) A 40 Hz train of 1 ms laser pulses reliably stimulates an action potential with every laser pulse over a 3 second period (top trace). A comparable train with a pulse frequency of 50 Hz, however, shows some stimuli failing to trigger action potentials toward the end of the pulse train. Following a “miss”, the subsequent action potential has increased amplitude due to decreased levels of both sodium channel inactivation and residual potassium channel conduction (bottom trace). (B) Trains of 1 ms optical stimuli (top trace) and electrical stimuli (bottom trace) produce similar results, with the cell missing a similar number of stimuli in each case. This suggests that the maximum firing rate we observe is a function of the cell itself, and not due to the optical stimulation technique. (C) Under voltage clamp, the capacitive currents observed as a result of a laser pulse appear virtually identical at 40 Hz (top trace) and 200 Hz (bottom trace). This implies that AuNP-mediated photostimulation may be viable at frequencies well beyond 40 Hz.

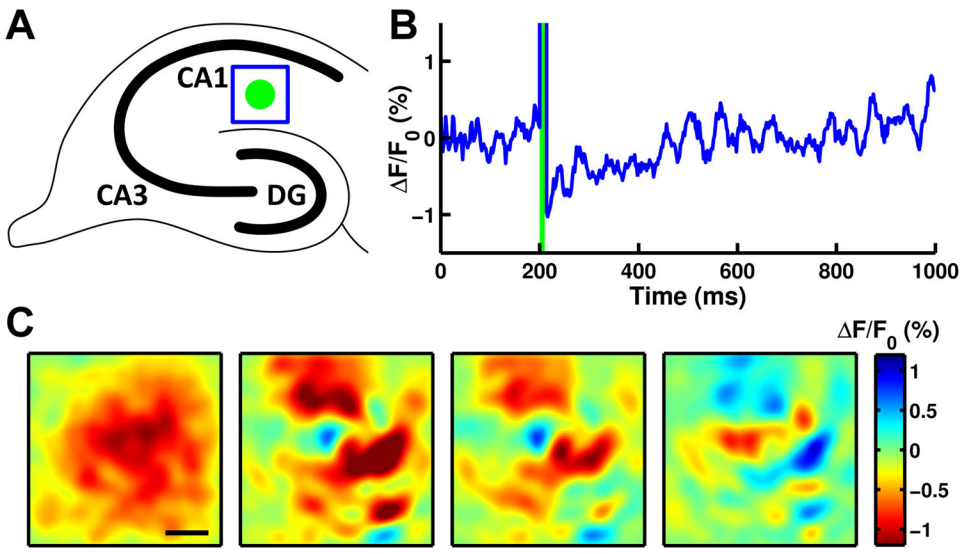

Figure 4.

AuNP-Ts1 enables all-optical electrophysiological investigation of mouse hippocampal slices. (A) Diagram of a mouse hippocampus showing the approximate location of the AuNP-Ts1 injection (green dot) and imaging region (blue square) in the CA1 region. CA3 and the dentate gyrus (DG) are also shown. (B) Fluorescence from the voltage-sensitive infrared dye ICG was used to monitor neuronal activity. The fluorescence decreases in response to a 532 nm optical stimulus (225 mW, 10 ms – green bar), indicating cellular depolarization. Recovery to baseline occurs over several hundred milliseconds. An artifactual spike is observed during the optical stimulus due to direct excitation of ICG with the 532 nm laser. (C) ICG is able to spatially resolve patterns of neural activity induced by the optical stimulus and track them over time as activity returns to baseline levels. A series of four baseline-subtracted images are shown, each showing the average activity over four consecutive 80 ms windows following the stimulus. The first window begins 20 ms after the start of the laser pulse (far left frame), while the others begin 100 ms, 180 ms, and 260 ms (far right frame) following the optical stimulus. The baseline image to subtract was created by averaging 180 ms of data from before the stimulus. The data in these images are from the same acquisition as in B. The scale bar in the first image is 100 μm. Gaussian image filtering has been applied to these images (see supplemental experimental procedures for details). See also Figure S4.

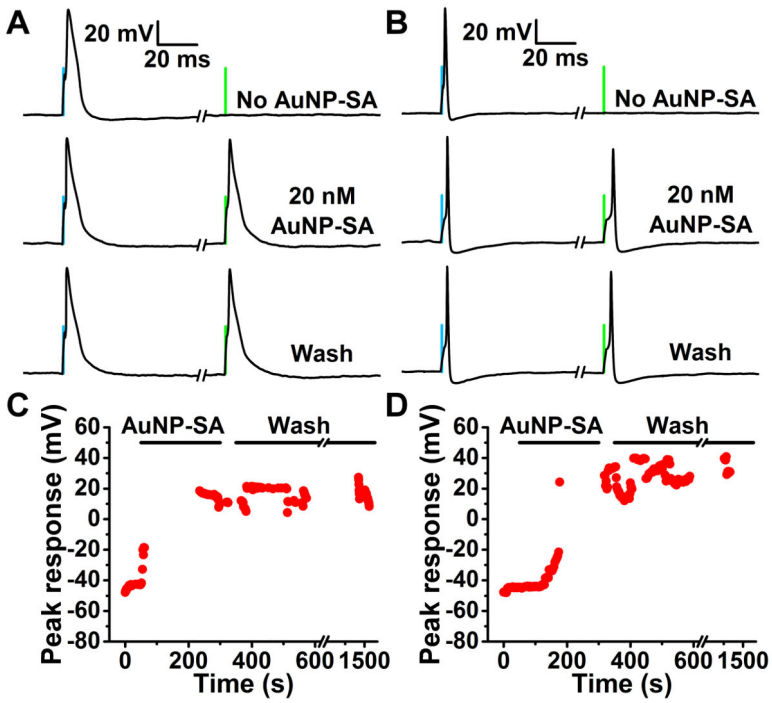

Figure 5.

Effects of AuNP-SA on biotinylated antibody-treated DRG neurons. (A,B) Streptavidin-functionalized AuNPs bound to biotinylated antibodies targeting both TRPV1 (A) and $P2X_3$ receptor (B) retain the ability to sensitize neurons to light. As with AuNP-Ts1 (Figure 2B), these conjugates are resistant to perfusion washout. Electrical stimuli (500 pA, 1 ms – blue bars) and optical stimuli (126 mW, 532 nm, 1ms – green bars) are shown. (C,D) Both anti-TRPV1 (C) and anti-$P2X_3$ receptor (D) keep AuNPs attached to neurons during 20 minutes of continuous forced fluid washing. See also Figures S5 and S6.

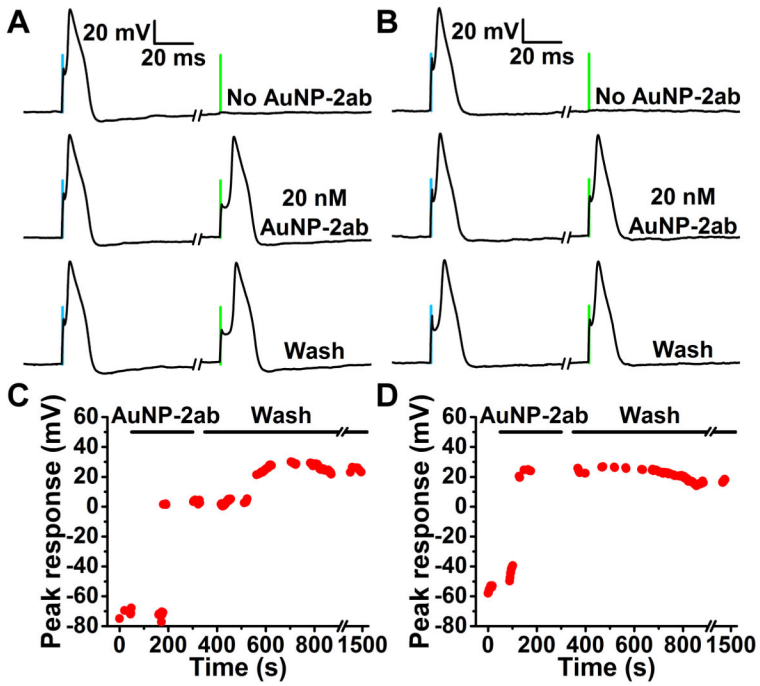

Figure 6.

Effects of AuNP-2abs on DRG neurons treated with unmodified primary antibodies. (A,B) AuNPs conjugated to secondary antibodies bind primary antibodies targeting both TRPV1 (A) and $P2X_3$ receptor (B). The AuNPs retain the ability to sensitize neurons to light. Electrical stimuli (500 pA, 1 ms – blue bars) and optical stimuli (126 mW, 532 nm, 1ms – green bars) are shown. (C,D) AuNP-2abs bound to both anti-TRPV1 (C) and anti-$P2X_3$ receptor (D) primary antibodies are highly resistant to active washout. Overall, the performance of AuNP-2abs bound to unmodified primary antibodies (shown in this figure) appears similar to that of AuNP-SAs bound to biotinylated primary antibodies (shown in Figure 5). See also Figures S5 and S6.

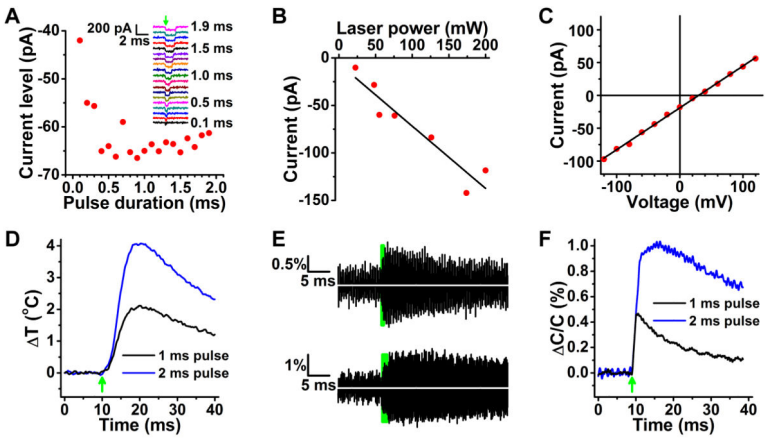

Figure 7.

AuNPs confer optical sensitivity to pure lipid bilayers. (A) Under voltage-clamp, 174 mW 532 nm laser pulses of increasing duration do not produce currents of increasing magnitude. Rather, as pulse duration increases, peak current amplitudes appear to quickly saturate. (*Inset*) Traces show that no decrease in current magnitude is evident over the durations tested. Holding potential is −60 mV. (B) Under voltage-clamp, optically-induced currents increase in magnitude with increasing laser power, showing a near-linear dependence. Holding potential is −60 mV, and laser pulse duration is 0.3 ms. (C) Laser-induced currents depend linearly on voltage-clamp holding potential, with reversal potential near 0 mV. Laser pulse duration is 0.3 ms. (D) Temperatures, measured with a micropipette at a short distance above the membrane, continue to increase long after the end of the laser pulses. Indicated temperatures are averages of data obtained with 300 traces. (E) Membrane capacitance was measured by calculating the impedance of the bilayer in response to a sinusoidal applied voltage. The sinusoidal current increases in response to a laser pulse, indicating an increase in capacitance. To emphasize changes in sine wave amplitude, only the peaks of the waves are shown. Green bars show optical stimuli. (F) After rectification and filtering, the changes in capacitance (verified by the phase shift in the impedance analysis) are made clear. Capacitance increases linearly during the laser pulses, then decays back to baseline after a delay (or even small continued increase) that depends nonlinearly on laser pulse duration. Capacitance traces are averages of two acquisitions. In all traces, green arrows show the starts of optical stimuli. See also Figures S7 and S8.